Available online at www.sciencedirect.com
ScienceDirect
Journal of Hazardous Materials 151 (2008) 682–691
Journal of Hazardous Materials
www.elsevier.com/locate/jhazmat

An investigation of Cu(II) adsorption by raw and acid-activated bentonite: A combined potentiometric, thermodynamic, XRD, IR, DTA study

E. Eren *, B. Afsin

Department of Chemistry, Faculty of Arts and Sciences, Ondokuz Mayis University, 55139 Kurupelit-Samsun, Turkey

Received 13 April 2007; received in revised form 12 June 2007; accepted 12 June 2007
Available online 16 June 2007

Abstract

Adsorption of Cu(II) by raw bentonite (RB) and acid-activated bentonite (AAB) samples was investigated as a function of the initial Cu(II) concentration, solution pH, ionic strenght, temperature, the competitive and complexation effects of ligands (Cl^-, SO_4^{2-}, PO_4^{3-}). Langmuir monolayer adsorption capacity of the RB (42.41 mg g^{-1}) was found greater than that of the AAB (32.17 mg g^{-1}). The effect of structural charges on the reactivity of the edge groups was evidenced by the particular proton adsorption behaviour of the bentonite samples. The spontaneity of the adsorption process is established by decrease in ΔG which varied from −0.34 to −0.71 kJ mol^{-1} (RB), −1.13 to −1.49 kJ mol^{-1} (AAB) in temperature range 303–313 K. Infrared (IR) spectra of the bentonite samples showed that the positions and shapes of the fundamental vibrations of the OH and Si–O groups were influenced by the adsorbed Cu(II) cations. Differential thermal analysis (DTA) results showed that adsorbed Cu(II) cations have a great effect on the thermal behaviour of the bentonite samples. The X-ray diffraction (XRD) spectra indicated that the Cu(II) adsorption onto the bentonite samples led to changes in unit cell dimensions and symmetry of the parent bentonites.

Keywords: Clay; Adsorption; Thermodynamic; Surface charge; Heavy-metal

1. Introduction

Heavy-metal pollution occurs in many industrial wastewater such as those produced by metal plating facilities, mining operations, battery manufacturing process, the production of paints and pigments, and the glass production industry. Due to their accumulation through food chain and persistent in nature, it is necessary to remove toxic heavy-metals from wastewater. Intake of excessively large doses of copper by man leads to severe mucosal irritation and corrosion, widespread capillary damage, hepatic and renal damage and central nervous system irritation followed by depression. Severe gastrointestinal irritation and possible necrotic changes in the liver and kidney could occur [1].

Conventional technologies for the removal of heavy-metal such as chemical precipitation, electrolysis, ion exchange and reverse osmosis are often neither effective nor economical. Among the physico-chemical treatment process adsorption is higly effective, cheap and easy to adapt [2]. Adsorption has been proven to be a successful method for removal of heavy metals from wastewater. Activated carbon is higly effective in adsorbing heavy metals from wastewater but high cost limits its use. The abundance of clay minerals and their low cost are a strong candidate as an adsorbent for removal of heavy-metal from wastewater. Because of their high specific surface area and exchange capacity, clay minerals also play a significant role in determining the availability and transport of metal species in soils and waters.

Bentonite is a natural clay mineral that is found in many places of the world. Any clay of volcanic origin that contains montmorillonite is referred to as bentonite. It belongs to the 2:1 clay family, the basic structural unit of which is composed of two tetrahedrally coordinated sheets of silicon ions surrounding a sandwiched octahedrally coordinated sheet of aluminum ions. The isomorphous substitution of Al^{3+} for Si^{4+} in the tetrahedral layer and Mg^{2+} or Zn^{2+} for Al^{3+} in the octahedral layer

* Corresponding author. Tel.: +90 362 312 19.
E-mail address: erdalern@omu.edu.tr (E. Eren).

0304-3894/$ – see front matter © 2007 Elsevier B.V. All rights reserved.
doi:10.1016/j.jhazmat.2007.06.040

results in a net negative surface charge on the clay [3]. Compared with other clay types, it has excellent sorption properties and possesses sorption sites available within its interlayer space as well as on the outer surface and edges [4]. Adsorption of metal ions onto montmorillonite appears to involve two distinct mechanism: (i) an ion exchange reaction at permanent charge sites, and (ii) formation of complexes with the surface hydroxyl groups [5,6].

IR spectroscopy has significantly contributed to the understanding of the structure, bonding, and reactivity of clay minerals [7–13]. The examination of the IR spectra (4000–400 cm^{-1}) provides information on fundamental vibrational modes of the constituent units of these materials. OH stretching and bending vibrations occur in the spectral region of 3750–3500 and 950–600 cm^{-1}, respectively. Si–O and Al–O stretching modes are found in the 1200–700 cm^{-1} range, while Si–O and Al–O bending modes dominate the 600–400 cm^{-1} region.

The objective of this study is to investigate comparative adsorption characteristics for removal of Cu(II) from aqueous solution by the use of RB and AAB. The influence of pH, ionic strength, ligands (Cl^-, SO_4^{2-}, PO_4^{3-}) and temperature on the adsorption of Cu(II) by the RB and AAB samples was investigated to better understand the Cu(II) adsorption process and the impact of metal and ligands on this process.

2. Experimental

2.1. Materials

Preparation of RB: The bentonite sample (from Unye, Turkey) was grounded and washed in deionized water several times at a 1:10 bentonite/water ratio. The mixture was stirred for 3 h and then kept standing overnight, followed by separation, washing and drying at 60 °C.

Preparation of AAB: The RB was treated under mechanical stirring with 2.0 M H_2SO_4 solution at 90 °C for 4 h in a two-necked glass flask under reflux. The mass ratio of the bentonite to the acid solution was 1:1. After activation the solids were washed by deionized water until SO_4^{2-} free, dried at 60 °C, and grounded to pass through a 78–120 μm size sieve.

Preparation of Cu(II)-saturated bentonites: 1 g of the bentonite sample and 100 mL of $Cu(NO_3)_2{\cdot}5H_2O$ solution (0.1 M) were used to obtain Cu(II)-saturated RB (Cu-RB) and Cu(II)-saturated AAB (Cu-AAB). The resulting mixtures were stirred for 7 day at pH ≈ 5, followed by seperation, washing and drying slowly at 60 °C.

2.2. Methods

2.2.1. Characterization procedures

The mineralogical compositions of the RB and AAB samples were determined from the XRD patterns of the products taken on a Rigaku 2000 automated diffractometer using Ni filtered Cu Kα radiation. XRD analysis of the montmorillonite was performed using the three-principal lines [14]. IR spectra of the bentonite samples were recorded in the region 4000–400 cm^{-1} on a Mattson-1000 FTIR spectrometer at 4 cm^{-1} resolution. Thermal analysis was performed simultaneously on a Rigaku TG 8110 thermal analyzer combined with TAS (Thermal Analysis System) 100 (range 25–1000 °C) under static air atmosphere at a heating rate of 10 °C min^{-1}. Calcined α-alumina was taken as a reference. Surface areas were measured by nitrogen adsorption at 77 K using Quantachromosorb. Moisture and gases on the solid surface or penetrated in the open pores were removed by heating at 120 °C for 2 h prior to the surface area measurements. The values determined for RB and AAB were 36.61 and 110.36 $m^2\ g^{-1}$, respectively.

The cation exchange capacities (CEC) of the samples were determined by the adsorption of Cu(II)–ethylene diamine complex [15]. The values of CEC for the RB and AAB were 15.87 and 8.89 mg Cu(II) g^{-1} bentonite, respectively.

Potentiometric titrations was made in 10^{-3}, 10^{-2} and 10^{-1} M solutions of NaCl, 0.4 g of the bentonite sample and 50 cm^{-3} of electrolyte solution were titrated in polyethylene vessels. The suspension was mixed with a magnetic stirrer. Prior to the titration the suspension was equilibrated under N_2 at its natural pH for 4 h. Following equilibration, the pH value was adjusted by adding of 0.1 M HCl solution. Suspension was then titrated by the addition of 0.1 M NaOH solution. After each addition of a small amount base, it was stable for 5 min and pH was recorded. To check reversibility, suspension was back titrated with 0.1 M HCl solution [16].

2.2.2. Cu(II) adsorption procedures

All reagents used were of analytical grade. Cu(II) adsorption studies were followed as described by Sarkar et al. [17,18]. A solution of 2.94 mM Cu(II) was prepared from $Cu(NO_3)_2{\cdot}5H_2O$ by dissolving in deionisied water. The stock was diluted to prepare a working solution of 2.94 μM Cu(II). The background electrolyte solutions were 0.01, 0.1 and 0.5 KNO_3. The experimental procedure involved the equilibration of 0.1 g bentonite sample in 24 mL of background electrolyte solution with 6 mL of Cu(II) working solution in 50 mL polyethylene centrifuge tubes. This resulted in concentrations of 3.3 g L^{-1} of solid and 0.6 μM Cu(II). Solution pH was adjusted with 0.1 M HNO_3 or 0.1 M NaOH, such that the equilibrium solutions had pH values ranging from 3.0 to 6.5. Preliminary kinetic studies indicated that Cu(II) adsorption was characterized by a rapid initial adsorption (within 1 h) followed by a much slower, continious uptake. A 24-h contacting period was found to be sufficient to achieve equilibrium. The separation of the liquid from the solid phase was achieved by centrifugation at 4500 rpm for 20 min. Adsorbed Cu(II) was calculated from the difference between the Cu(II) initially added to the system and that remaining in the solution after equilibration by a Unicam 929 model flame atomic absorption spectrophotometer. The dilutions induced by the pH controls were considered while computing the amount of Cu(II) adsorbed. Cu(II) adsorption in the presence of Cl^-, SO_4^{2-}, and PO_4^{3-} was performed by equilibrating 0.1 g of bentonite in 21 mL of 0.1 M KNO_3 background electrolyte, 6 mL of Cu(II) working solution, and 3 mL of a NaCl, Na_2SO_4, or a Na_2HPO_4 working solution (achieveing 0.01 M Cl^-, 0.01 M SO_4^{2-}, or 0.01 M PO_4^{3-}) in 50-mL polyethylene centrifuge tubes. These experiments were performed in duplicate.

Table 1
Chemical composition of the samples

Sample	SiO_2 (%)	Al_2O_3 (%)	Fe_2O_3 (%)	CaO (%)	MgO (%)	Na_2O (%)	K_2O (%)
RB	62.70	20.10	2.16	2.29	3.64	0.27	2.53
AAB	67.15	17.20	1.66	1.69	3.14	0.15	1.78

3. Results and discussion

3.1. Adsorbent characterization

3.1.1. Chemical analysis

The chemical compositions of the RB and AAB samples was given in Table 1. The sample obtained after acid treatment showed a decrease in Al, Mg and Fe (octahedral cations) and an enrichment in SiO_2 coming from the tetrahedral layer of the montmorillonite and from the impurities of insoluble silicates (quartz and mica). These results indicate that the octahedral cations pass into the solution while silica, owing to its insolubility in acid solution, remains in the sample.

3.1.2. Surface properties of bentonite samples

In electrolyte solutions of NaCl, the interaction of the H^+ and OH^- ions with the bentonite surface was reflected in the shift of the titration curves. The surface charge is calculated from the potentiometric titration curves according to the relationship:

$$\sigma_H = \frac{F(C_a - C_b + [OH^-] - [H^+])}{mS} \quad (1)$$

where σ_H is the surface charge density ($C\,m^{-2}$), F the Faraday constant ($C\,mol^{-1}$), C_a and C_b the concentrations ($mol\,dm^{-3}$) of the acid and base added to the suspension $[OH^-]$ and $[H^+]$ the concentration of OH^- and H^+ measured from the pH of the solution, m the mass of the bentonite sample in the solution ($g\,dm^{-3}$), and S is the specific surface area of the sample ($m^2\,g^{-1}$).

Figs. 1 and 2 show proton adsorption curves (σ_H versus pH) performed at different supporting electrolyte concentrations for the RB and AAB samples. The main difference between the RB and AAB systems is the effect of electrolyte concentration on the pH_0 value where σ_H becomes zero. This value decreased by increasing the electrolyte concentration in the case of RB but were not change in the case of AAB. These results show that although the net charge at the edge surface of the RB is zero at pH_0, the net potential is negative because of the presence of structural charges [19–21]. This potential becomes less negative by increasing the electrolyte concentration and thus pH_0 decreases by increasing electrolyte concentration. As shown in Fig. 2, any change in the electrolyte concentration does not change the surface potential and consequently pH_0 is independent on the electrolyte concentration [19]. This result shows the decrease of structural charges due to the leached of aluminium ions in the tetrahedral layer and/or magnesium ions in the octahedral layers of montmorillonite, which has been confirmed in the next sections (Sections 3.2.1 and 3.2.2) by XRD, IR spectra and chemical analysis results.

3.2. Location of cations in Cu(II)-adsorbed bentonite samples

3.2.1. X-ray diffraction studies of Cu(II) adsorbed onto bentonite samples

For the XRD pattern of RB, one reflection was observed in the region $2^\circ < 2\theta < 8^\circ$. This corresponds to the 5.76° (2θ) value from which the interlamellar distance was found to be 15.33 Å. For the XRD pattern of the AAB, the formation of a porous structure was observed by the shoulder appearing in the region $2^\circ < 2\theta < 8^\circ$ (Fig. 3). The X-ray pattern of AAB sample indicated a slight shift in the position of d_{001} peak from 15.33 to 16.98 Å which was accompained by a decrease in intensity from 100 to 68% (Table 2). The XRD pattern of AAB show poor crystallinty,

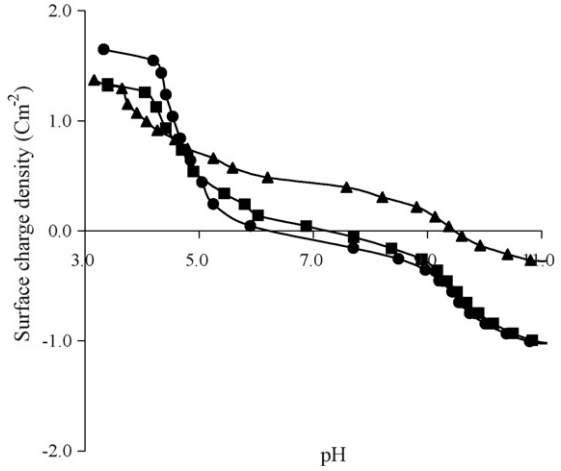

Fig. 1. σ_H (C/m^2) vs. pH curves of RB in NaCl solutions: triangles, 1.0 M; squares, 0.1 M; circles, 0.01 M.

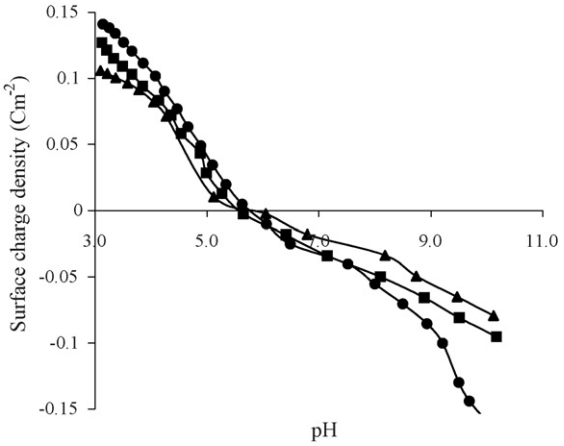

Fig. 2. σ_H (C/m^2) vs. pH curves of AAB in NaCl solutions: triangles, 1.0 M; squares, 0.1 M; circles, 0.01 M.

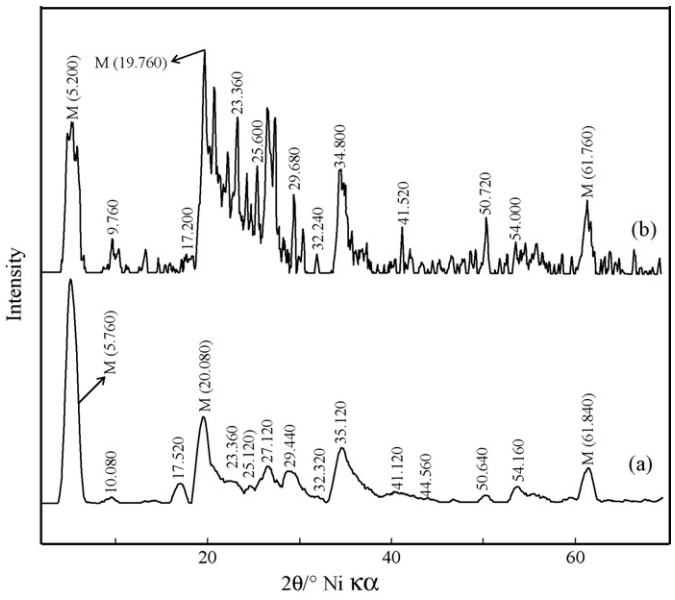

Fig. 3. The XRD patterns of the RB (a) and AAB (b) (M: montmorillonite).

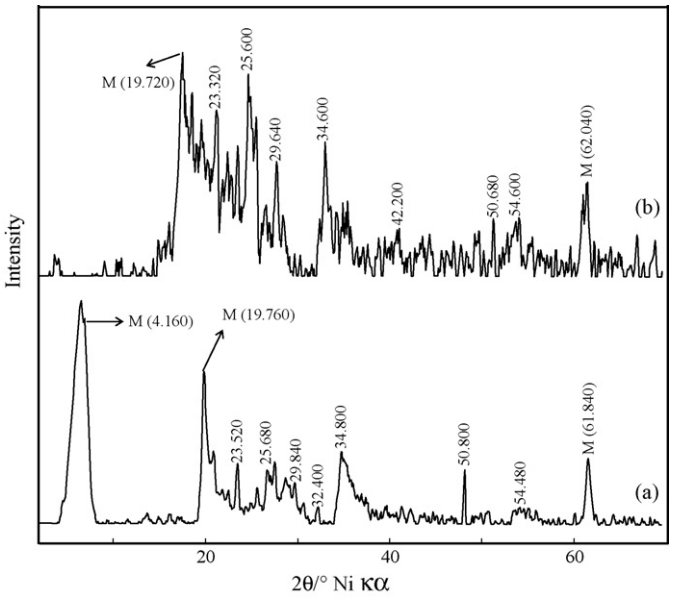

Fig. 4. The XRD patterns of the Cu-RB (a) and Cu-AAB (b) (M: montmorillonite).

broad and less intense peaks compared to the parent clay mineral due to the presence of layers activated with hydrogen ions, or an irregular stacking of activated and non-activated layers and thus the structure of the resultant clay becomes amorphous to XRD.

The XRD patterns of the Cu(II)-saturated RB and AAB samples are shown in Fig. 4 and the details of the reflection positions and intensities are reported in Table 2. Several reflections were observed in the region $2^\circ < 2\theta < 8^\circ$ for the patterns of the Cu(II)-saturated bentonite samples. One reflection situated at a higher 2θ value corresponds to the basal spacing, the other reflections situated at a lower 2θ values are likely to appear because of the agglomeration of clay sheets [22,23]. The adsorption of Cu(II) onto the RB and AAB samples led to decrease in the basal spaces of the host materials from 15.33 and 16.98 to 13.97 and 12.91 Å, respectively. The intensities gain in Cu-RB and Cu-AAB is approximately 1.33 and 1.19 fold higher than in their host materials counterparts. Both types of the bentonites showed almost identical differences in terms of their XRD patterns upon Cu(II) adsorption. These differences indicate the effects of Cu(II) adsorption on the stucture of clay minerals, and are not sample-specific. The XRD spectra of Cu-RB and Cu-AAB indicated that the Cu(II) adsorption may lead to changes in unit cell dimensions and symmetry of the parent bentonites. Also, the Bragg angle for several reflections has notably changed, while for others it essentially remained same. These findings show that Cu(II) cations are arranged in one or more equivalent positions and they contribute to the reflection intensities. The intensity of basal spacing peak at 6.84° (2θ) for the Cu-AAB is much weaker than that for the AAB. This finding shows that the basic structure of AAB was nearly collapsed during the Cu(II) adsorption.

3.2.2. IR spectra studies of Cu(II) adsorbed onto bentonite samples

The XRD and IR spectra of RB indicate that montmorillonite is the dominant mineral phase in this clay (Figs. 3 and 5a). The absorption band at 3635 cm^{-1} is due to stretching vibrations of structural OH groups of montmorillonite. The bands corresponding to AlAlOH, AlFeOH and AlMgOH bending vibrations were observed at 936, 885 and 845 cm^{-1}, respec-

Table 2
d-Spacing and relative intensity for bentonite samples

RB											
d (Å)	15.33	4.41	3.80	3.54	3.28	3.03	2.76	2.55	2.19	1.69	1.49
I/I_0	100	40	10	8	18	16	4	26	6	8	16
AAB											
d (Å)	16.98	4.48	3.80	3.56	3.23	3.00	2.77	2.57	2.17	1.69	1.50
I/I_0	68	100	72	32	70	36	10	48	22	16	34
Cu-RB											
d (Å)	13.97	4.48	3.93	3.46	3.31	2.99	2.76	2.57	2.39	1.68	1.49
I/I_0	100	68	16	18	24	20	8	32	12	8	30
Cu-AAB											
d (Å)	–	4.46	3.81	3.63	3.34	3.01	2.58	2.41	1.80	1.62	1.50
I/I_0	–	56	72	38	98	82	38	16	22	14	32

tively. A complex band at 1038 cm^{-1} is related to the stretching vibrations of Si–O groups, while the bands at 527 and 470 cm^{-1} are due to Al–O–Si and Si–O–Si bending vibrations, respectively. The band at 629 cm^{-1} was assigned to coupled Al–O and Si–O out-of-plane vibrations. Water in montmorillonite gave a broad band at 3415 cm^{-1} corresponding to the H_2O-stretching vibrations, with a shoulder near 3330 cm^{-1}, due to an overtone of the bending vibration of water observed at 1651 cm^{-1} [11].

The changes in the Si environment after acid activation process were reflected in both the position and the shape of the Si–O stretching band near 1038 cm^{-1}. A slight shift of this band to higher frequencies indicates alteration of the structure. The IR spectrum of the AAB (Fig. 5b) shows, in addition to the tetrahedral Si–O band near 1063 cm^{-1}, absorption band at 1114 cm^{-1}, assigned to Si–O vibrations of amorphous silica with a three-dimensional framework [7]. The spectrum of the AAB sample, has all absorption bands characteristics of amorphous silica (1114, 808 and 476 cm^{-1}) confirms a high degree of structural decomposition (Fig. 5b).

Detailed analysis of IR spectra in the whole spectral region (4000–400 cm^{-1}) can be use for discern of the location of Cu(II) cations [8,10]. The structural modifications of the tetrahedral and octahedral sheets due to the adsorbed Cu(II) cations influenced the fundamental vibrations of the Si–O and OH groups (Fig. 5c and d). For example, the stretching OH band was shifted up to 3643 cm^{-1} and moreover, a new band appeared near 3514 cm^{-1} in the spectra of all Cu(II)-saturated bentonite samples. This band, assigned to AlMgCuOH vibration, confirms the presence of the Cu(II) ions in the former vacant octahedral sites. The IR patterns of the Cu(II)-saturated bentonite samples showed a strong broad band of water near 3463 and 3438 cm^{-1} for the RB and AAB samples, respectively, due to the overlapping asymmetric ν_3 and symmetric ν_1 (H–O–H) stretching vibrations and the absorption near 1635 cm^{-1} related to the ν_2 (H–O–H) bending vibrations (Fig. 5c and d). The band of RB at 3361 cm^{-1} was ascribed to an overtone ($2\nu_2$) of the bending mode [24]. The broad band near 1038 cm^{-1}, assigned to complex Si–O stretching vibrations in the tetrahedral sheet, upon saturation process moved to 1049 cm^{-1} for the RB sample (Fig. 5c). The position of the Si–O bending vibration at 527 cm^{-1}, due to Si–O–Al remained basically unchanged for the Cu(II)-saturated samples, but some broadening and a decrease in intensity of the Si–O–Al band were observed (Fig. 5c and d).

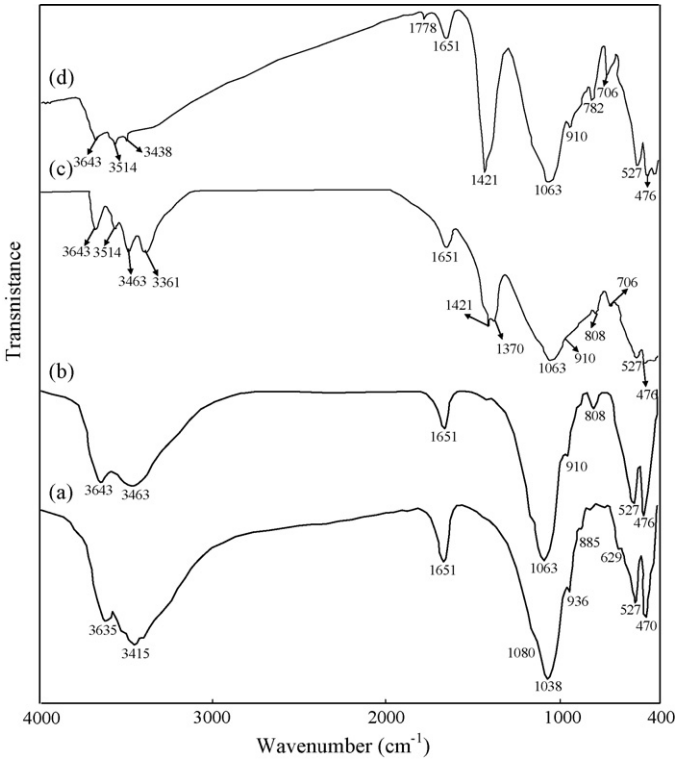

Fig. 5. IR spectra of the RB (a), AAB (b), Cu-RB (c), and Cu-AAB (d).

3.2.3. Thermal analysis study of the Cu(II) adsorbed onto bentonite samples

The curve related to the RB exhibited mass losses by 5.80 and 5.50% in temperature ranges 20–200 and 200–700 °C, respectively (Fig. 6a). The two endothermic peaks in the DTA curve of RB in the range of 20–200 °C denote the release of different water species coordinated to the interlayer cations and surface humidity. Especially, the second endothermic peak at about 150 °C represents stronger hydrogen bonding between water molecules and exchangeable cations. The third endother-

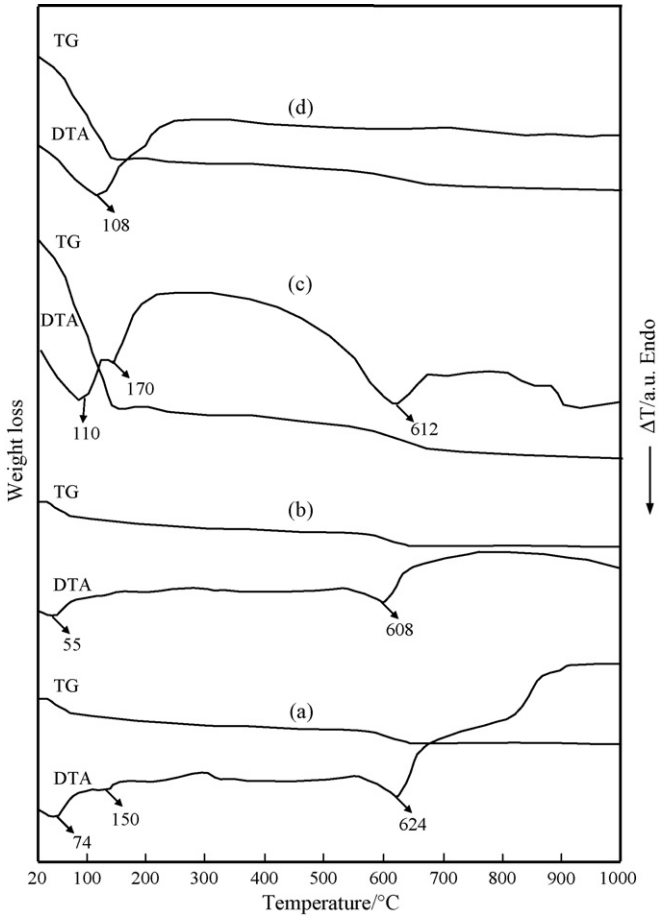

Fig. 6. Thermal analysis curves of the RB (a), AAB (b), Cu-RB (c), and Cu-AAB (d).

mic peak centered at 624 °C were related to the dehydroxylation of the layer silicate minerals. The curve relating to the AAB sample exhibited mass loss 6.85% at 20–200 °C and 2.43% at 200–680 °C, which due to the thermal evolution of moisture and interlayer water, and structural OH groups, respectively (Fig. 6b). The DTA curve of Cu-RB showed two endothermic peaks about 110 and 170 °C, related to the water molecules bound to the interlayer cations (Fig. 6c). The examination of DTA curves for the RB and Cu-RB samples indicates that the dehydroxylation of Cu-RB occurs at low temperature (612 °C) as compared to RB sample (624 °C), revealing the stronger interaction between OH and the Cu(II) ions, and a different composition of the octahedral sheet after Cu(II) adsorption [25,26]. This result show that the structure of the dehydroxylation product depends on the acidity of the adsorbed Cu(II) cation [27,28]. The dehydroxylation peak of Cu-AAB in temperature range 600–700 °C was not showed due to the dehydroxylation process started at low temperature (Fig. 6d). Because the dehydroxylation process may be catalysed by protons originating from water coordinated to the Cu(II) cation, and thus dehydroxylation could started before the complete evolution of water [27,28].

3.3. Adsorption of Cu(II) by bentonite samples

3.3.1. Adsorption model

The Langmuir and Freundlich isotherm models were applied to establish the relationship between the amounts of Cu(II) adsorbed by the RB and AAB bentonite samples. The experimental data conformed to the linear form of Langmuir model [29] expressed as the following equation:

$$\frac{C_e}{q_e} = \frac{C_e}{q_m} + \frac{1}{K_L q_m} \quad (2)$$

where C_e is the equilibrium concentration of metal (mg L^{-1}), q_e the amount of the metal adsorbed (mg) by per unit of bentonite (g), and q_m and K_L are the Langmuir constant related to adsorption capacity (mg g^{-1}) and the energy of adsorption (L g^{-1}), respectively. q_m and K_L constant were evaluated from slope and intercept of the linear plots of C_e/q_e versus C_e, respectively (Fig. 7). It is well known that Langmuir monolayer adsorption capacity (q_m) gives the amount of Cu(II) required to occupy all the available sites in unit mass of the bentonite samples. The Langmuir monolayer adsorption capacities for RB and AAB were found as 32.17 and 42.41 mg g^{-1}, respectively. This result can be conclude that the adsorption of Cu(II) over these samples could not be modeled by only a cation exchange reaction, since adsorbed amount of Cu(II) seem to be higher than the CECs of the bentonite samples (the values of CEC for the RB and AAB were 15.87 and 8.89 mg Cu(II) g^{-1} bentonite, respectively). Thus, the Cu(II) adsorption is occurred not only ion exchange in exchangeable cations, but also specific adsorption, which can be described by surface complexation model which define a reaction between functional surface groups and Cu(II) ions [30–32]. The Langmuir equilibrium coefficient, b, related to the equilibrium constant of the process. The lower b value for the AAB (0.01 L g^{-1}) compared to the RB (0.20 L g^{-1}) indicate that acid activation process influenced the Cu(II) adsorption equilibrium.

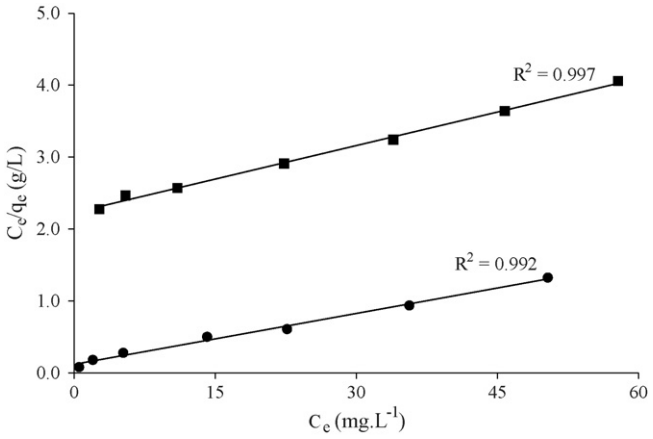

Fig. 7. Linear plots of Langmuir isotherms of Cu(II) adsorption on bentonite samples: circle, RB; squares, AAB.

The Freundlich adsorption isotherm is applicable to the adsorption on heterogeneous clay surfaces. The adsorption equilibrium data was applied to the Freundlich model in logaritmic form [33] given as follows:

$$\log q_e = \log K_f + \frac{1}{n}\log C_e \quad (3)$$

where K_f and n are Freundlich constants related to adsorption capacity and adsorption intensity, respectively. K_f and $1/n$ were determined from the intercept and slope of linear plot of $\log q_e$ versus $\log C_e$, respectively (Fig. 8).

The Freundlich plots have good linearity for both the bentonite samples ($r^2 = 0.990$ and 0.997) at 298 K (Fig. 8). The values of the adsorption coefficients, computed from Freundlich plots are given in the Table 3. The adsorption intensity given by the Freundlich coefficient ($1/n$) is smaller than 1 (these values for the RB and AAB are 0.42 and 0.82, respectively) for both the bentonite samples, and indicating that the adsorption of Cu(II) onto bentonite samples under studied conditions is favorable. The Freundlich adsorption capacity (K_f) was

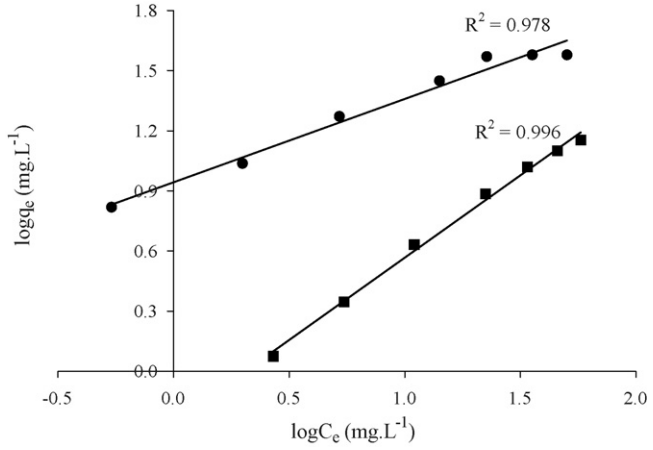

Fig. 8. Linear plots of Freundlich isotherms of Cu(II) adsorption on bentonite samples: circle, RB; squares, AAB.

Table 3
Adsorption isotherm constants for the adsorption of Cu(II) onto bentonite samples (q_m: mmol/g, K_L: L/mol, K_f: mmol$^{(1-1/n)}$ L$^{1/n}$/g)

Sample	Langmuir model			Freundlich model		
	q_m	K_L	r^2	$1/n$	K_f	r^2
RB	32.17	0.20	0.992	0.42	8.77	0.990
AAB	42.41	0.01	0.996	0.82	0.55	0.997

found to be 8.77 and 0.55 for the RB and AAB samples, respectively.

3.3.2. Effect of ionic strength and pH

The adsorption of Cu(II) onto the bentonite samples as a function of ionic strength and pH was shown in Fig. 9a and b. Both the bentonite samples showed an identical behaviour of increased adsorption of Cu(II) per unit mass with gradually increasing pH, and the shape of curves dependent on the bentonite surfaces. As shown in Fig. 9a, Cu(II) adsorption by the RB sample decreased when pH decreased. This result suggest that the adsorptive decrease was caused by the competition for exchange sites between hydrogen and Cu(II) cations. At below pH 5.0 there is also a decrease in Cu(II) adsorption with increasing ionic strength. This can be explained by competition of Cu(II) cations with the background cation potasium at the face sites [34]. With increasing pH, an increasing fraction of Cu(II) was sorbed onto edge sites and the effect of the background electrolyte concentration on Cu(II) adsorption decreased [31,34]. The adsorption of Cu(II) onto the RB appears to involve two distinct mechanism: (1) the interlayer of montmorillonite through ion exchange reaction at permanent charge sites are responsible for cation uptake at in the range $3 < pH < 5$. This assertion is based on the following experimental evidence: (i) Cu(II) cations are sorbed by RB at low pH values, and (ii) the adsorption of Cu(II) at these low pH values is strongly influenced by ionic strength. (2) The Cu(II) forms surface complexes with silanol and aluminol groups at the edges of the crystals at $pH > 5$. Thus, sorption of Cu(II) onto RB sample can be described by two reactions. The first involves formation of outer-sphere complexes via cation exchange reactions at the permanent negatively charges at faces and/or interlayer regions of montmorillonite. The second reaction occurs above pH 5 and involves formation of an inner-sphere surface Cu(II)-hydroxy surface complex at variable-charge surface hydroxyl groups.

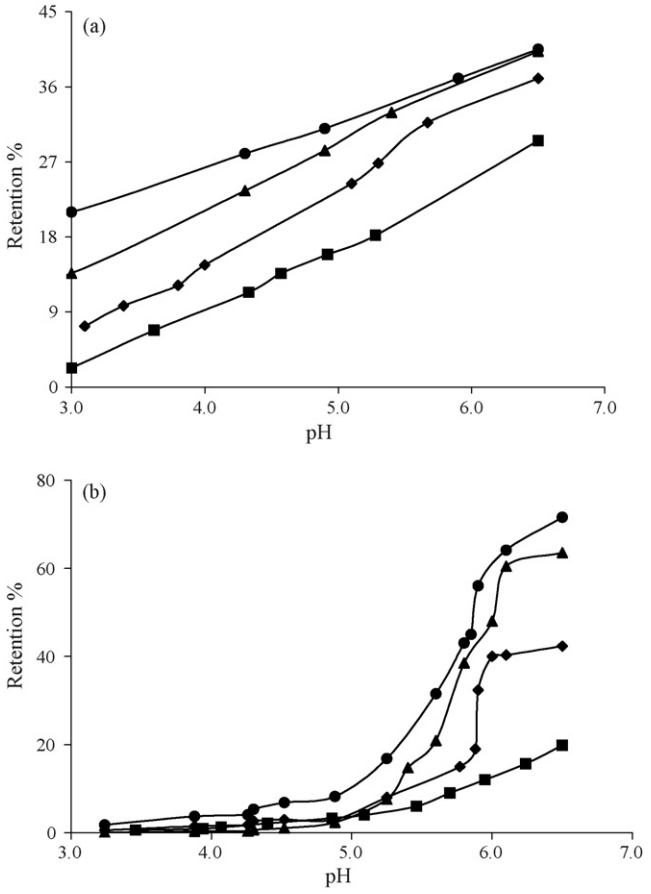

Fig. 9. Adsorption of Cu(II) (0.6 μM) by (a) RB and (b) AAB (3.3 g L^{-1}) as function of pH and ionic strenght (IS) (controlled by KNO_3): squares, 1.0 M; diamonds, 0.1 M; triangles, 0.05 M; circles, 0.02 M.

The adsoption curve of AAB have a different shape from that of RB sample, and the adsorption capacity of AAB is higher than that of RB (Fig. 9b). The adsoption curve for this sample is characterized by two distinct adsorption edges. For example, in the presence of 0.1 M KNO_3, the first stage of adsorption edge commenced about 2% Cu(II) adsorption at pH ∼ 3.0 and ended at pH ∼ 5.0, at which about 5% of the total Cu(II) had been adsorbed. The second stage started at pH 5.0 and continued up to pH 6.5 where about 44% of the total Cu(II) was adsorbed. The uptake of Cu(II) within the pH range 3.0–5.0 is not highly influenced by ionic strength. As shown in the Section 3.1.2, the shape of the cation adsorption curve for AAB suspension does not change with increasing ionic strength of the medium (due to the removed exchangeable cations such as Ca, Mg and Fe). This behaviour is thought to result from decreased amounts of permanent negative charges inside the clay particle (due to isomorphic substitution) and the pH-dependent charges on the edges (due to acid–base reactions of surface groups). If the presence of the mentioned negative charges originates a net negative potential at the edges, they can change their effective affinity of edge groups for cations when the ionic strength is changed [21]. Because this negative charge becomes less negative by increasing the ionic strength. Thus, decreased permanent charge of the AAB may also affect not only adsorption edge, but also surface complexation of Cu(II) cations on the edges.

3.3.3. Effect of inorganic ligands

The adsorption of Cu(II) by the bentonite samples was influenced by the presence of Cl^-, SO_4^{2-} and PO_4^{3-} (Fig. 10a and b). While it is clear that aqueous speciation influences Cu(II) adsorption in the inorganic ligand systems, the mechanism by which ligands impact Cu(II) retention depends on the surface type. The adsorbed Cu(II) in the presence of inorganic ligands may be also attributed to a high specifity of the surfaces for Cu(II) relative to ligands.

The percent Cu(II) adsorbed in the 0.01 M Cl^- systems at pH 6.0 are 58 and 48% for the RB and AAB samples, compared

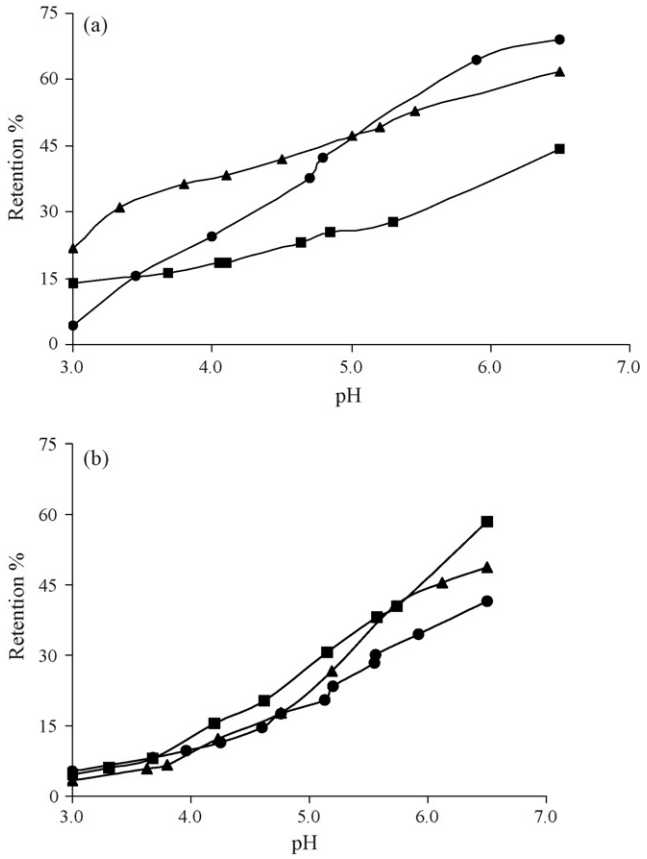

Fig. 10. Adsorption of Cu(II) (0.6 μM) by (a) RB and (b) AAB (3.3 g L^{-1}) as function of pH and in the presence of Cl^-, SO_4^{2-}, and PO_4^{3-} [ionic strenght (IS) is 0.1 M (KNO_3); circles, PO_4^{3-}; squares, SO_4^{2-}; triangles, Cl^-].

to 32 and 40% at the same pH but in the absence of Cl^-. The increased amount of adsorbed Cu(II) can be explained in terms of solution chemistry. Because, Cu–Cl, CuOH–Cl complexes are the dominate Cu(II) species in the presence of 0.01 M Cl^-. The enhanced retention of Cu(II) by bentonite surfaces in the presence of 0.01 M PO_4^{3-} may also suggest that the observed Cu(II) adsorption behaviour in the bentonite suspensions is influenced by both aqueous speciation and surface phosphate complexation of Cu(II) ions [17,18,35,36]. The reduction in Cu(II) adsorption on the RB sample in the presence 0.01 M SO_4^{2-} might be due to sulfate ion competition with the various Cu(II) species for adsorption sites {e.g. [XOH^+–SO_4^{2-}] and [XOH^+–SO_4H^+] [17,18,37,38]}. Also, the reduced retention of Cu(II) in the presence of SO_4^{2-} may be explained through the formation of basic Cu(II)–SO_4^{2-} complexes {e.g. [CuOH–SO_4]$^-$ and [$Cu(OH)_2$–SO_4]$^{2-}$}.

3.3.4. Thermodynamic studies

Using the following equations, the thermodynamic parameters of the adsorption process were determined from the experimental data:

$$\ln K_d = \frac{\Delta S}{R} - \frac{\Delta H}{RT} \quad (4)$$

$$\Delta G = \Delta H - T\Delta S \quad (5)$$

$$K_d = \frac{C_a}{C_e} \quad (6)$$

where K_d is the distribution coefficient for the adsorption; ΔS, ΔH and ΔG are the changes of entropy, enthalpy and the Gibbs energy, respectively; T (K) is the temperature; R (J mol^{-1} K^{-1}) the gas constant, C_e (mmol L^{-1}) the equilibrium adsorbate concentration in the aqueous phase and C_a (mmol L^{-1}) is the amount of Cu(II) adsorbed per unit mass of the adsorbent. The values of ΔH and ΔS were determined from the slopes and intercepts of the plots of $\ln K_d$ versus $1/T$ (not showed). The distribution coefficient (K_d) indicates the capability of clay to retain a solute and also the extent of its movement in a solution phase [39]. According to Gomes et al. [40], K_d is a useful parameter for comparing the adsorption capacities of different clays or materials for any particular ion, when measured under the same experimental conditions.

The negative values for the Gibbs free energy change, ΔG, show that the adsorption process for the two bentonite samples is spontaneous and the degree of spontaneity of the reaction increases with increasing tempreature. The values of ΔG are less negative for the AAB, suggesting that the adsorption process for this material is more spontaneous. These results suggest that the internal domains of this sample are more suitable environments for Cu(II) cations than the RB sample. The data shown in Table 4 show that the heats of adsorption are positive for both types of the bentonite samples. These positive values of ΔH indicate the endothermic behaviour of the adsorption reaction of Cu(II) ions and suggest that a large amount of heat is consumed to transfer the Cu(II) ions from aqueous into the solid phase. As was suggested by Nunes and Airoldi [41], the transition metal ions must give up a larger share of their hydration water before they could enter the smaller cavities. Such a release of water from the divalent cations would result in positive values of ΔS. This mechanism of the adsorption of Cu(II) ions is also supported by the positive values of ΔS, which show that Cu(II) ions are less hydrated in the bentonite layers than in the aqueous solution. Also, the positive value of ΔS indicates the increased disorder in the system with changes in the hydration of the adsorbing Cu(II) cations.

Table 4
Thermodynamic parameters for the adsorption of Cu(II) onto bentonite samples

Sample	ΔH (kJ mol^{-1})	ΔS (J mol^{-1} K^{-1})	ΔG (kJ mol^{-1})			r^2
			303.15	313.15	323.15	
RB	10.36	42.0	−0.34	−0.52	−0.71	0.99
AAB	4.29	18.0	−1.13	−1.31	−1.49	0.99

4. Conclusions

The adsorption of Cu(II) by bentonite samples was influenced by pH, ionic strenght, and the presence of Cl^-, SO_4^{2-}, PO_4^{3-}. The adsorption of Cu(II) by the bentonite samples is a complex process controlled by a number of environmental variables. The isotherm studies suggest that Cu(II) sorption onto the RB sample occurs in two stages. The first stage involves adsorption on permanent charge sites and the second involves adsorption on variable charge sites. The adsorption capacity of the RB (15.87 mg Cu(II) g^{-1} bentonite) was much greater than that of the AAB (8.89 mg Cu(II) g^{-1} bentonite). This behaviour is related to the higher cation exchange and H^+ adsorption capacities of the RB with respect to the AAB. The endothermic nature of the proceses can be accounted for by the partial dehydration of Cu(II) before its sorption on the bentonite samples. Generaly, the ligands enhanced Cu(II) retention, perhaps by the surface complexation of Cu(II) species by specifically adsorbed ligands that resulted in a bridging surface complex. The presence of Cl^- and PO_4^{3-} increased Cu(II) adsorption by the RB, however, the presence of SO_4^{2-} also decreased the Cu(II) adsorption. The presence of Cl^-, SO_4^{2-} and PO_4^{3-} increased Cu(II) adsorption by the AAB. The findings require confirmation by direct methods such as extended X-ray absorption fine structure (EXAFS). IR studies showed that Cu(II) cations replaced the original metal ions in the interlayer or locate into hexagonal cavities of Si–O sheet in the Cu(II)-saturated bentonite samples. Structural modification of tetrahedral sheets due to the presence of Cu(II) cations either in hexagonal holes and/or in the previously vacant octahedral sites induces changes in the Si–O vibration modes. The lower dehydroxylation temperature values for the Cu(II)-saturated bentonite samples than the parent materials showed the higher dehydroxylation rate, and the decomposed bentonite structure.

References

[1] M. Ajmal, A.H. Khan, S. Ahmad, A. Ahmad, Role of sawdust in the removal of copper(II) from industrial wastes, Water Res. 32 (1998) 3085–3091.

[2] A.K. Bhattacharya, S.N. Mandal, S.K. Das, Adsorption of Zn(II) from aqueous solution by using different adsorbents, Chem. Eng. J. 123 (2006) 43–51.

[3] P.F. Luckham, S. Rossi, The colloidal and rheological properties of bentonite suspensions, Adv. Colloid Interface Sci. 82 (1999) 43–92.

[4] A. Tabak, B. Afsin, S.F. Aygun, E. Koksal, Structural charactristics of organo-modified bentonites of different origin, J. Therm. Anal. Calorim. 87 (2007) 375–381.

[5] O. Abollino, M. Aceto, M. Malandrino, C. Sarzanini, E. Mentasti, Adsorption of heavy metals on Na-montmorillonite, Effect of pH and organic substances, Water Res. 37 (2003) 1619–1627.

[6] E. Álvarez-Ayuso, A. García-Sánchez, Removal of heavy metals from waste waters by natural and Na-exchanged bentonites, Clays Clay Miner. 51 (2003) 475–480.

[7] J. Madejová, J. Bujdák, M. Janek, P. Komadel, Comparative FT-IR study of structural modifications during acid treatment of dioctahedral smectites and hectorite, Spectrochim. Acta A 54 (1998) 1397–1406.

[8] J. Madejová, B. Arvaiová, P. Komadel, FTIR spectroscopic characterization of thermally treated Cu^{2+}, Cd^{2+}, and Li^+ montmorillonites, Spectrochim. Acta A 55 (1999) 2467–2476.

[9] J. Madejová, M. Janek, P. Komadel, H.J. Herbert, H.C. Moog, FTIR analyses of water in MX-80 bentonite compacted from high salinary salt solution systems, Appl. Clay Sci. 20 (2002) 255–271.

[10] J. Madejová, H. Pálková, P. Komadel, Behaviour of Li^+ and Cu^{2+} in heated montmorillonite: evidence from far-, mid-, and near-IR regions, Vib. Spectrosc. 40 (2006) 80–88.

[11] J. Madejová, FTIR techniques in clay mineral studies, Vib. Spectrosc. 31 (2003) 1–10.

[12] W.P. Gates, P. Komadel, J. Madejová, J. Bujdák, J.W. Stucki, R.J. Kirkpatrick, Electronic and structural properties of reduced-charge montmorillonites, Appl. Clay Sci. 16 (2000) 257–271.

[13] P. Komadel, J. Madejová, J.W. Stucki, Structural Fe(III) reduction in smectites, Appl. Clay Sci. 34 (2006) 88–94.

[14] R.W. Grimshaw, The Chemistry and Physics of Clays, Ernest Benn Ltd., London, 1971, pp. 968–979.

[15] F. Bergaya, M. Vayer, CEC of clays: measurement by adsorption of a copper ethylenediamine complex, Appl. Clay Sci. 12 (1997) 275–280.

[16] G. Atun, G. Hisarli, A study of surface properties of red mud by potentiometric method, J. Colloid Interface Sci. 228 (2000) 40–45.

[17] D. Sarkar, M.E. Essington, K.C. Misra, Adsorption of mercury(II) by variable charge surfaces of quartz and gibbsite, J. Am. Soil Sci. Soc. 63 (1999) 1626–1636.

[18] D. Sarkar, M.E. Essington, K.C. Misra, Adsorption of mercury(II) by kaolinite, J. Am. Soil Sci. Soc. 64 (2000) 1968–1975.

[19] M.J. Avena, Acid–base behaviour of clay surfaces in aqueous media, Enc. Surf. Colloid Sci. (2002) 37–63.

[20] M.J. Avena, C.P. De Pauli, Proton adsorption and electrokinetics of an Argentinean montmorillonite, J. Colloid Interface Sci. 202 (1998) 195–204.

[21] M.J. Avena, M.M. Mariscal, C.P. De Pauli, Proton binding at clay surfaces in water, Appl. Clay Sci. 24 (2003) 3–9.

[22] G. Szöllösi, A. Mastalir, M. Bartok, Effect of ion exchange by an organic cation on platinum immobilization on clays, React. Kinet. Catal. Lett. 74 (2001) 241–249.

[23] D. Dermatas, M.S. Dadachov, Rietveld quantification of montmorillonites in lead-contaminated soils, Appl. Clay Sci. 23 (2003) 245–255.

[24] J.L. Bishop, C.M. Pieters, J.O. Edwards, Infrared spectroscopic analyses on the nature of water in montmorillonite, Clays Clay Miner. 42 (1994) 702–716.

[25] H.P. He, J.G. Guo, X.D. Xie, J.L. Peng, Location and migration of cations in Cu^{2+}-adsorbed montmorillonite, Environ. Int. 26 (2001) 347–352.

[26] Z. Ding, R.L. Frost, Study of copper adsorption on montmorillonites using thermal analysis methods, J. Colloid Interface Sci. 269 (2004) 296–302.

[27] S. Yariv, Ir evidence for migration of protons in H-montmorillonites and organo-montmorillonites, Clays Clay Miner. 21 (1973) 199.

[28] V. Balek, Z. Malek, S. Yariv, G. Matuschek, Characterization of montmorillonite saturated with various cations, J. Therm. Anal. Cal. 56 (1999) 67–76.

[29] I. Langmuir, The adsorption of gases on plane surfaces of glass, mica and platinum, J. Am. Soc. 40 (1918) 1361–1403.

[30] S. Nir, G. Rytwo, U. Yermiyahu, L. Margulies, A model for cation adsorption to clays and membranes, Colloid Polym. Sci. 272 (1994) 619–632.

[31] A.M.L. Kraepiel, K. Keller, F.M.M. Morel, A model for metal adsorption on montmorillonite, J. Colloid Interface Sci. 210 (1999) 43–54.

[32] C.H. Weng, C.Z. Tsai, S.H. Chu, Y.C. Sharma, Adsorption characteristics of copper(II) onto spent activated clay, Sep. Purif. Technol. 54 (2007) 187–197.

[33] H. Freundlich, Über die adsorption in lösungen, Zeitschrift für Physikalische Chemie (Leipzig) 57 385–470.

[34] I. Heidmann, I. Christl, C. Leu, R. Kretzschmar, Competitive sorption of protons and metal cations onto kaolinite: experiments and modeling, J. Colloid Interface Sci. 282 (2005) 270–282.

[35] S. Mustafa, A. Naeem, S. Murtaza, N. Rehana, H.Y. Samad, Comparative sorption properties of metal(III) phosphates, J. Colloid Interface Sci. 220 (1999) 63–74.

[36] A. Naeem, S. Mustafa, N. Rehana, B. Dilara, S. Murtaza, The sorption of divalent metal ions on $AlPO_4$, J. Colloid Interface Sci. 252 (2002) 6–14.

[37] P.J. Swedlund, J.G. Webster, Cu and Zn ternary surface complex formation with SO_4^{2-} on ferrihydrite and schwertmannite, Appl. Geochem. 16 (2001) 503–511.

[38] K.O. Adebowale, I.E. Unuabonah, B.I. Olu-Owolabi, Adsorption of some heavy metal ions on sulfate- and phosphate-modified kaolin, Appl. Clay Sci. 29 (2005) 145–148.

[39] M.R. Reddy, S.J. Dunn, Distribution coefficients for nickel and zinc in soils, Environ. Pollut. 11 (1986) 303–313.

[40] P. Gomes, M. Fontes, A.G. Silva, E.S. Mendonça, A.R. Metto, Selectivity sequence and competitive adsorption of heavy metals by Brazilian soils, Soil Sci. Soc. Am. 65 (2001) 1115–1121.

[41] L.M. Nunes, C. Airoldi, Some features of crystalline α-titanium hydrogenphosphate, modified sodium and *n*-butylammonium forms and thermodynamics of ionic exchange with K^+ and Ca^{2+}, Thermochim. Acta 328 (1999) 297–305.